Relativistic tight-binding calculation of core-valence transitions in Pt and Au

L. F. Mattheiss and R. E. Dietz
Bell Laboratories, Murray Hill, New Jersey 07974
(Received 28 March 1980)

The results of a relativistic tight-binding energy-band model for Pt and Au, utilizing parameters derived from Smith's empirically adjusted combined interpolation scheme, are applied to calculate the one-electron contribution to various x-ray and energy-loss spectra involving $4f$ and $2p$ core states in these materials. These results show that the unoccupied holes in the Pt $5d$ bands have predominantly $j = 5/2$ character ($h_{5/2}$) such that the ($h_{5/2}/h_{3/2}$) ratio ranges from ~ 3.5 within 0.5 eV of E_F to ~ 2.9 over the entire unoccupied conduction band. Taking into account dipole transition probabilities, the former ratio leads to a predicted line-strength ratio $I_{N_7}/I_{N_6} \approx 2.9$ near threshold for excitations involving the $4f\,j = 7/2$ (N_7) and $j = 5/2$ (N_6) core levels in Pt. This result is in good agreement with the corresponding experimental ratios that are derived from electron energy-loss (2.5) and x-ray-absorption (2.3) spectra. Comparable agreement is obtained between the calculated and observed (electron-energy-loss) I_{N_7}/I_{N_6} ratios in Au. The present results are applied to calculate the N_6–N_7 x-ray emission spectra in both Pt and Au and to interpret the L_2–L_3 absorption-edge data in Pt.

I. INTRODUCTION

Core-excitation spectra in the heavier metals and their compounds provide a novel technique for probing the total-angular-momentum character $j = l \pm \frac{1}{2}$ of either filled (x-ray emission) or empty (x-ray absorption, electron energy loss) conduction-band states. This possibility was first proposed by Mott[1] to explain an unusual feature in the L absorption spectrum of Pt. Namely, it was observed by Cauchois and Manescu[2] that the L_3 edge in Pt contains a "white line" or sharp peak in the absorption coefficient while the L_2 edge does not. Mott noted that if the $5d$ holes in Pt were predominantly states with $j = \frac{5}{2}$, then one would expect transitions from the L_3 ($j = \frac{3}{2}$) but not from the L_2($j = \frac{1}{2}$) core states because of the atomic dipole selection rule $\Delta j = 0, \pm 1$.

The first attempt to confirm Mott's idea involved a tight-binding calculation by Brown *et al.*[3] which included only the Pt $5d$ energy-band states. Though these authors obtained a quantitative explanation of the observed difference in the L_2 and L_3 absorption edges in Pt, their calculated ratio of $j = \frac{5}{2}$ to $j = \frac{3}{2}$ holes $h_{5/2}/h_{3/2} \approx 14$ was in apparent conflict with much smaller estimates of this ratio which were derived from electron-energy-loss and soft-x-ray-absorption measurements[4] involving the $4f$ (N_6–N_7) core states.

The purpose of the present investigation is to show that a relativistic tight-binding band model for Pt, involving $5d$, $6s$, and $6p$ orbitals, can provide a consistent interpretation of core-level transitions involving both the $2p$ (L_2–L_3) and $4f$ (N_6–N_7) core states. The present study utilizes energy-band results that are derived from the Slater–Koster linear-combination-of-atomic-orbitals (LCAO) interpolation scheme.[5] The LCAO parameters for these calculations are determined by a fit to Smith's[6] empirically adjusted combined-interpolation-scheme band structure for Pt. The effects of dipole transition probabilities are included in these calculations by means of a sum rule which relates the emission intensity or absorption coefficient to a sum of terms involving angular momentum projected densities of states $N_{lj}(E)$.[7,8] The coefficient of each term in this sum involves a numerical factor and a radial dipole-moment integral. Estimates of the latter, based on nonrelativistic Herman–Skillman[9] atomic wave functions, show that the $5d$ contribution to the L_2–L_3 absorption spectra dominates that of the $6s$ states.

The results of the present calculations for Pt demonstrate that, because of hybridization with the broad $6s$-$6p$ bands, the calculated ratio $h_{5/2}/h_{3/2}$ is reduced substantially from that estimated previously in simplified LCAO model calculations involving only the Pt $5d$ bands.[3,4] The present $h_{5/2}/h_{3/2}$ ratio of ~3 is quite similar to that obtained recently by Christensen[10] using a relativistic generalization of the linear-muffin-tin-orbital method. In particular, the calculated ratio for holes within 0.5 eV of E_F $h_{5/2}/h_{3/2} \approx 3.5$ yields a predicted N_7 to N_6 line-strength ratio $I_{N_7}/I_{N_6} \approx 2.9$, which agrees well with values derived from electron-energy-loss (2.5) and x-ray-absorption (2.3) data.[4,11]

It is also shown that a reduced $h_{5/2}/h_{3/2}$ ratio of ~3 is consistent with the observed difference in the L_2–L_3 absorption edges in Pt.[3] Namely, if one applies the same general procedure as adopted by Brown *et al.*[3] to calculate the total absorption due to the integrated difference between the L_2 and L_3 edges, then excellent agreement is obtained between the theoretical and experimentally de-

rived estimates of the total absorption. It is concluded that this general procedure is relatively insensitive to the unoccupied conduction-band $h_{5/2}/h_{3/2}$ ratio.

Analogous calculations have also been carried out for Au. Though the $5d$ bands in Au are nominally filled, hybridization effects with the overlapping $6s$-$6p$ bands shift about 0.4 $5d$ holes above E_F with $h_{5/2}/h_{3/2} \approx 2.4$. This yields a predicted line-strength ratio $I_{N_7}/I_{N_6} \approx 2.1$ for $4f$ core excitations in Au. This ratio is in good agreement with the value that is extracted from electron-energy-loss data.

The organization of this paper is as follows. In Sec. II we describe the essential details of the present relativistic LCAO energy-band model for Pt and Au. In addition, we summarize the results of a general sum rule which relates interband transition probabilities to projected densities of states $N_{lj}(E)$ in cases where either the initial or final state is a relativistic core level. The LCAO energy-band results of the present calculations are presented in Sec. III. Section IV includes a discussion of the $N_{6,7}$ emission, absorption, and electron energy-loss spectra of Pt and Au as well as the $L_{2,3}$ absorption spectrum of Pt. Section V summarizes the conclusions that are obtained in this study.

II. COMPUTATIONAL DETAILS

A. LCAO band model

The present calculations apply the standard Slater–Koster LCAO interpolation scheme[5] for the fcc structure, with the energy parameters $E_{\alpha,\beta}(\vec{r})$ treated in their most general three-center form. Only nearest-neighbor d-d interactions were included in this treatment, and Smith's empirical values (E_0, Δ, A_1–A_6 in Table II of Ref. 6) were utilized. The remaining s-s, s-p, s-d, p-p, and p-d interaction parameters were determined by means of a nonlinear least-squares fit to Smith's empirically adjusted combined-interpolation-scheme band structure for Pt and Au. Interactions out to third neighbors were included in this fit, which involved a total of 35 LCAO parameters (including Smith's eight d-band parameters).

The fitting procedure was carried out at a total of 13 inequivalent points in the Brillouin zone and yielded an rms error of 0.01 Ry for the six lowest bands. Spin-orbit effects were included for the $5d$ states by means of an additional parameter ζ_{5d}, for which the Herman–Skillman atomic estimate[9] was used. Spin-orbit effects were neglected for the $6p$ orbitals, since the corresponding bandwidth is much greater than ζ_{6p}.

Using vector coupling coefficients,[12] it is straightforward to transform the LCAO $5d$ orbitals into states which are characterized by $j = l \pm \frac{1}{2}$ and $-j \leq m \leq j$. If the LCAO wave function for the νth band is written

$$\psi_{\nu\vec{k}} = \sum_{ljm} C^{\nu\vec{k}}_{ljm} \phi_{ljm}(\vec{r}), \tag{1}$$

then $N^{\nu\vec{k}}_{lj} = \sum_m |C^{\nu\vec{k}}_{ljm}|^2$ yields that fraction of the charge density that is associated with the lj subband. The LCAO band model provides both the band energies $E_{\nu\vec{k}}$ and the wave-function coefficients $C^{\nu\vec{k}}_{ljm}$. These allow one to calculate the density of states $N(E)$,

$$N(E) = \frac{2}{(2\pi)^3} \sum_\nu \int d^3k\, \delta(E - E_{\nu\vec{k}}), \tag{2}$$

as well as a projected density of states

$$N_{lj}(E) = \frac{2}{(2\pi)^3} \sum_\nu \int d^3k\, N^{\nu\vec{k}}_{lj} \delta(E - E_{\nu\vec{k}}). \tag{3}$$

As shown in the following section, a knowledge of $N_{lj}(E)$ is sufficient for a semiquantitative understanding of spectra involving core-level transitions.

The Brillouin-zone integrations that are involved in evaluating $N(E)$ and $N_{lj}(E)$ in Eqs. (2) and (3) have been carried out using the tetrahedral method.[13] For these calculations, the irreducible $\frac{1}{48}$ of the Brillouin zone was subdivided into 500 tetrahedra. This provided sufficient accuracy and energy resolution for the purposes of the present investigation. Furthermore, the resulting $N(E)$ curves are in good qualitative agreement with those of Smith *et al.*,[14] which were derived from his empirical combined-interpolation-scheme band structure.[6]

B. Transition probabilities

It has been shown[7,8] that the general expression for the relativistic emission or absorption intensity involving a core state with quantum numbers $n'l'j'$ ($j' = l' \pm \frac{1}{2}$) can be simplified to the form

$$I_{n'l'j'}(\omega) \propto (2j'+1) \sum_{lj} A^{n'l'j'}_{lj}(E) N_{lj}(E) \tag{4}$$

for dipole transitions. In the case of emission, the right-hand side of Eq. (4) contains an additional factor $(\hbar\omega)^3 = (E - E_{n'l'j'})^3$ which is omitted here for convenience. The coefficients $A^{n'l'j'}_{lj}(E)$ are slowly varying functions of energy so that any abrupt structure in $I_{n'l'j'}(\omega)$ arises solely from the projected conduction-band density of states $N_{lj}(E)$. These correspond to occupied states in the case of emission spectra and unoccupied or hole states in the case of absorption. The dipole selection rule ($\Delta l = \pm 1$, $\Delta j = 0, \pm 1$) limits the sum over l and j to a maximum of three terms. This is shown explicitly in the general expression for $A^{n'l'j'}_{nl}(E)$,[8]

$$A_{lj}^{n'l'j'}(E)=\frac{1}{4}\left(\frac{1}{(j'+1)}\delta_{l,l'+1}\delta_{j,j'+1}+\frac{1}{j'(j'+1)(2j'+1)}\delta_{l,l'+1}\delta_{jj'}+\frac{1}{j'}\delta_{l,l'-1}\delta_{j,j'-1}\right)[R_{lj}^{n'l'j'}(E)]^2, \quad (5)$$

where $R_{jl}^{n'l'j'}(E)$ is the radial dipole-moment integral

$$R_{lj}^{n'l'j'}(E)\equiv\int_0^R r^3 R_{n'l'j'}(r)R_{lj}(r,E)dr. \quad (6)$$

The energy dependence in $A_{lj}^{n'l'n'}(E)$ originates from that contained in the radial conduction-band wave functions $R_{lj}(r,E)$. Unlike the relativistic augmented-plane-wave (APW) and Korringa-Kohn-Rostoker (KKR) methods,[15] the present Slater-Koster LCAO scheme assumes energy-independent conduction-band wave functions. Furthermore, the radial wave functions are undetermined by this scheme.

In the present study, we have used approximate values for the radial dipole integrals in Eq. (6). We have estimated these using the appropriate nonrelativistic Herman-Skillman atomic wave functions. In evaluating these integrals, we have renormalized the atomic functions to unity within a Wigner-Seitz volume and set R in Eq. (6) equal to the Wigner-Seitz radius $R_{\rm WS}$.

In order to illustrate the individual terms that occur in Eq. (4) for $I_{n'l'j'}(\omega)$, we summarize the nonvanishing coefficients $(2j'+1)A_{lj}^{n'l'j'}$ in Table I for core and conduction-band states with s, p, d, and f symmetry. Each row (column) of this table corresponds to a core (valence) state with quantum numbers $n'l'j'$ (lj). As an example, we consider the emission or absorption intensity $I_{N_6}(\omega)$ and $I_{N_7}(\omega)$ that result from $4f$ core-electron excitations with $j'=\frac{5}{2}$ (N_6) and $j'=\frac{7}{2}$ (N_7), respectively. Neglecting conduction-band states with g-type symmetry, we find

$$I_{N_6}(\omega)\propto\tfrac{1}{35}(R_{d_{5/2}}^{4f_{5/2}})^2N_{d_{5/2}}(E)+\tfrac{21}{35}(R_{d_{3/2}}^{4f_{5/2}})^2N_{d_{3/2}}(E),$$
$$I_{N_7}(\omega)\propto\tfrac{20}{35}(R_{d_{5/2}}^{4f_{7/2}})^2N_{d_{5/2}}(E). \quad (7)$$

If we consider the case of absorption and neglect the energy dependence of the radial-dipole integrals, then the integrated N_6 and N_7 intensities I_{N_6} and I_{N_7} can be expressed in terms of the $j=\frac{5}{2}$ ($h_{5/2}$) and $j=\frac{3}{2}$ ($h_{3/2}$) holes in the d band, where

$$h_j=\int_{E_F}^{\infty}N_{dj}(E)dE. \quad (8)$$

In particular, neglecting differences in the radial-dipole integrals, the ratio of these integrated intensities is given by

$$I_{N_7}/I_{N_6}=20h_{5/2}/(h_{5/2}+21h_{3/2}). \quad (9)$$

According to the results in Table I, the analogous expression for the ratio of the integrated L_3 and L_2 absorption intensities [involving $2p$ core states with $j'=\frac{3}{2}$ (L_3) and $j'=\frac{1}{2}$ (L_2), respectively] is

$$I_{L_3}/I_{L_2}=(6h_{5/2}+h_{3/2})/5h_{3/2}, \quad (10)$$

provided that one neglects transitions to unoccupied s-type conduction-band states (as, for example, Brown *et al.*[3] assume). These expressions, Eqs. (9) and (10), will be used in subsequent discussions.

One can derive similar relations for the case of

TABLE I. Values of $(2j'+1)A_{lj}^{n'l'j'}/(R_{lj}^{n'l'j'})^2$ for core (columns) and conduction (rows) electron quantum numbers $n'l'j'$ and lj, respectively.

$\frac{(2j'+1)A_{lj}^{n'ljj'}}{(R_{lj}^{n'l'j'})^2}$		s	p		d		f	
		$j=\frac{1}{2}$	$j=\frac{3}{2}$	$j=\frac{1}{2}$	$j=\frac{5}{2}$	$j=\frac{3}{2}$	$j=\frac{7}{2}$	$j=\frac{5}{2}$
$n's'$	$j'=\frac{1}{2}$		$\frac{1}{3}$	$\frac{1}{3}$				
$n'p'$	$j'=\frac{3}{2}$	$\frac{2}{3}$			$\frac{6}{15}$	$\frac{1}{15}$		
	$j'=\frac{1}{2}$	$\frac{1}{3}$			0	$\frac{5}{15}$		
$n'd'$	$j'=\frac{5}{2}$		$\frac{9}{15}$	0			$\frac{5}{35}$	$\frac{1}{35}$
	$j'=\frac{3}{2}$		$\frac{1}{15}$	$\frac{10}{15}$			0	$\frac{14}{35}$
$n'f'$	$j'=\frac{7}{2}$				$\frac{20}{35}$	0		
	$j'=\frac{5}{2}$				$\frac{1}{35}$	$\frac{21}{35}$		

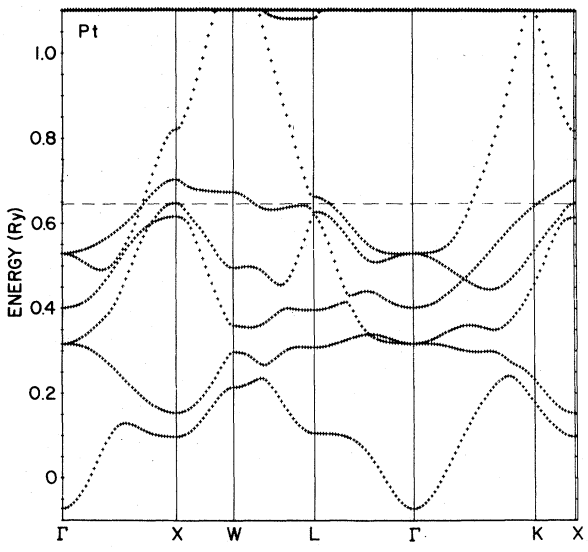

FIG. 1. LCAO bands for Pt along symmetry lines in the Brillouin zone.

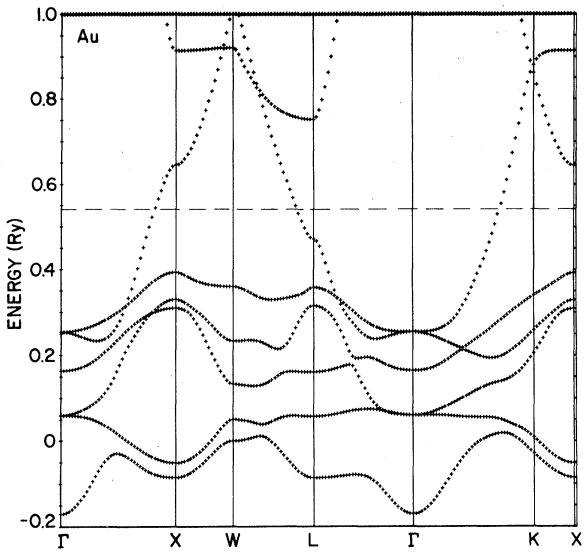

FIG. 2. LCAO bands for Au along symmetry lines in the Brillouin zone.

the integrated x-ray emission intensities by taking $N_{tj}(E)$ in Eq. (4) to be the occupied conduction-band states. In the case of d bands, Eq. (8) is replaced by

$$n_j = \int_{E_m}^{E_F} N_{dj}(E)dE\,, \tag{11}$$

where E_m is the conduction-band minimum and $n_j + h_j = 2j + 1$. The intensity ratios for emission, assuming a statistical occupation of the initial core-hole excited states (see Sec. IV for a discussion of this point), can be found from Eqs. (9) and (10) by making the substitution $h_j \to n_j$.

III. RESULTS

The present LCAO energy-band results[16] for Pt and Au are plotted along symmetry lines in the Brillouin zone in Figs. 1 and 2, respectively. These results involve the Herman–Skillman[9] atomic $5d$ spin-orbit parameters $\zeta_{5d} = 0.046$ Ry (Pt) and $\zeta_{5d} = 0.053$ Ry (Au). In each figure, the Fermi energy E_F is indicated by the dashed horizontal line.

The accuracy of the present LCAO fit to Smith's semiempirical combined-interpolation scheme results[6] is confirmed by a detailed comparison between the two sets of band profiles. Equally good agreement is exhibited between these LCAO bands and the results of first-principles relativistic-augmented-plane-wave (RAPW) calculations for Pt (Ref. 17) and Au.[18]

The corresponding LCAO density-of-states curves for Pt and Au are shown in Figs. 3 and 4, respectively. In these figures, the solid curve represents the total density of states $N(E)$, while the dashed and dotted curves correspond to the projected $5d$ $j = \frac{5}{2}$ $[N_{d_{5/2}}(E)]$ and $j = \frac{3}{2}$ $[N_{d_{3/2}}(E)]$ components. In both cases, the total density-of-states curves are in excellent agreement with previously published results for Pt (Refs. 14 and 19) and Au.[10,14,18] Equally good agreement is also obtained between the projected $N_{d_{5/2}}(E)$ and $N_{d_{3/2}}(E)$ components shown in Figs. 3 and 4 and the rela-

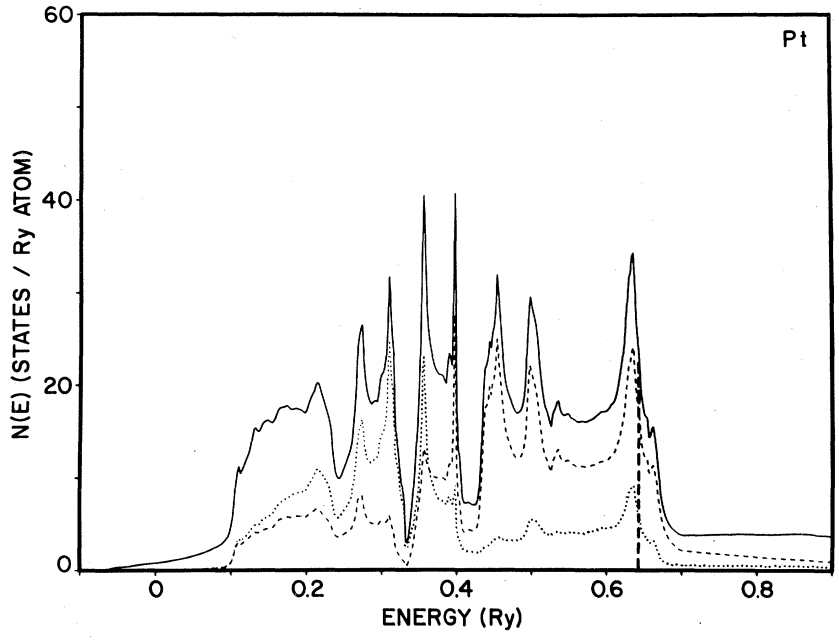

FIG. 3. LCAO density of states $N(E)$ (solid line) for Pt, including $N_{d_{5/2}}(E)$ (dashed) and $N_{d_{3/2}}(E)$ (dotted) components.

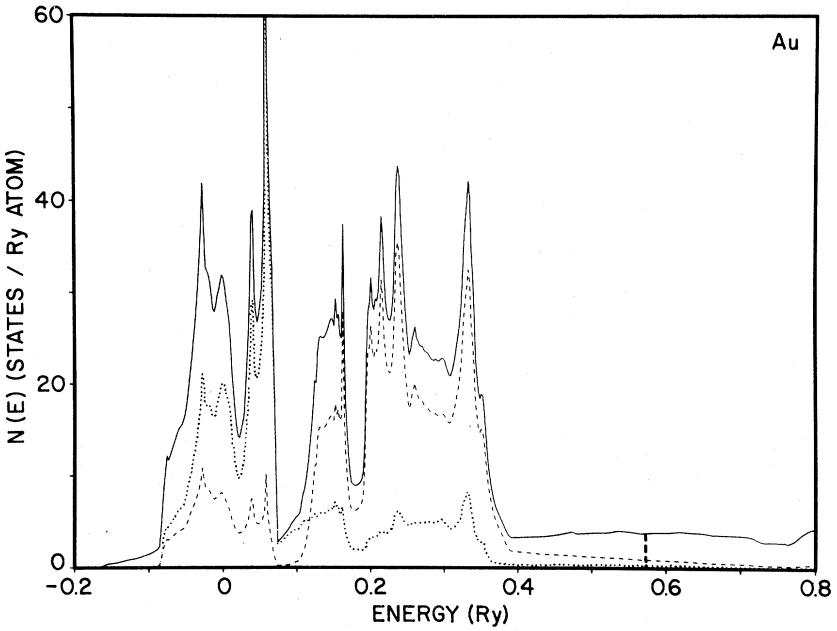

FIG. 4. LCAO density of states $N(E)$ (solid line) for Au, including $N_{d_{5/2}}(E)$ (dashed) and $N_{d_{3/2}}(E)$ (dotted) components.

tivistic linear-muffin-tin-orbital (LMTO) results of Christensen.[10]

It is clear that the projected densities of states $N_{d_{5/2}}(E)$ and $N_{d_{3/2}}(E)$ must be proportional to one another in the ratio $\frac{6}{4}$ in the nonrelativistic limit where the spin-orbit parameter $\zeta_d \to 0$. Obviously, the results shown in Figs. 3 and 4 correspond to the opposite limit where the atomic d spin-orbit splitting $E_{so} = 5\zeta_d/2$ is comparable to the d-band width w_d. As discussed by Christensen,[10] these spin-orbit effects are predominant among the $5d$-series elements and play a diminished role for elements in the $4d$ and $3d$ transition series.

For convenience, we have summarized in Table II the integrals of the projected densities of states $N_{lj}(E)$, namely, the s, p, and d ($j = \frac{5}{2}, \frac{3}{2}$) electron densities n_s, n_p, $n_{d_{5/2}}$, and $n_{d_{3/2}}$, respectively. The corresponding hole densities h_{lj} can be obtained from the relation $n_{lj} + h_{lj} = 2j + 1$. It is found that in Pt, the ratio $h_{5/2}/h_{3/2} = 2.9$. This agrees well with the corresponding ratio $h_{5/2}/h_{3/2} = 3.3$ which is obtained from the LMTO results of Christensen. Similar agreement is obtained for the values of the density of states at E_F. Christensen quotes the results $N(E_F) = 23.2$, $N_{d_{5/2}}(E_F) = 16.0$, and $N_{d_{3/2}}(E_F) = 6.8$ states/Ry atom, while the corresponding LCAO values are $N(E_F) = 24.5$, $N_{d_{5/2}}(E_F) = 17.5$, and $N_{d_{3/2}}(E_F) = 6.1$ states/Ry atom.

As noted earlier, these values for the $h_{5/2}/h_{3/2}$ ratio in Pt are significantly smaller than previous estimates[3,4] which were obtained from simplified tight-binding models involving only the Pt $5d$

TABLE II. Summary of LCAO results for Pt and Au. The electron density n (electrons/unit cell) is decomposed into s, p, and d ($j = \frac{5}{2}, \frac{3}{2}$) components. The d ($j = \frac{5}{2}, \frac{3}{2}$) hole densities include those for the entire unoccupied conduction band ($h_{5/2}, h_{3/2}$) and an energy interval $\Delta = 0.5$ eV above E_F ($h^{\Delta}_{5/2}, h^{\Delta}_{3/2}$). The integrated intensity ratios I_{N_7}/I_{N_6} and I_{L_3}/I_{L_2} are evaluated using Eqs. (9) and (10), respectively.

	Pt	Au
E_F(Ry)	0.642	0.534
n_s	0.765	0.890
n_p	0.580	0.511
$n_{d_{5/2}}$	5.000	5.717
$n_{d_{3/2}}$	3.656	3.883
$h_{5/2}$	1.000	0.283
$h_{3/2}$	0.344	0.118
$h_{5/2}/h_{3/2}$	2.9	2.4
I_{N_7}/I_{N_6}	2.4	2.1
I_{L_3}/I_{L_2}	3.7	3.1
$h^{\Delta}_{5/2}$	0.372	0.036
$h^{\Delta}_{3/2}$	0.106	0.012
$h^{\Delta}_{5/2}/h^{\Delta}_{3/2}$	3.5	3.0
$I^{\Delta}_{N_7}/I^{\Delta}_{N_6}$	2.9	2.6

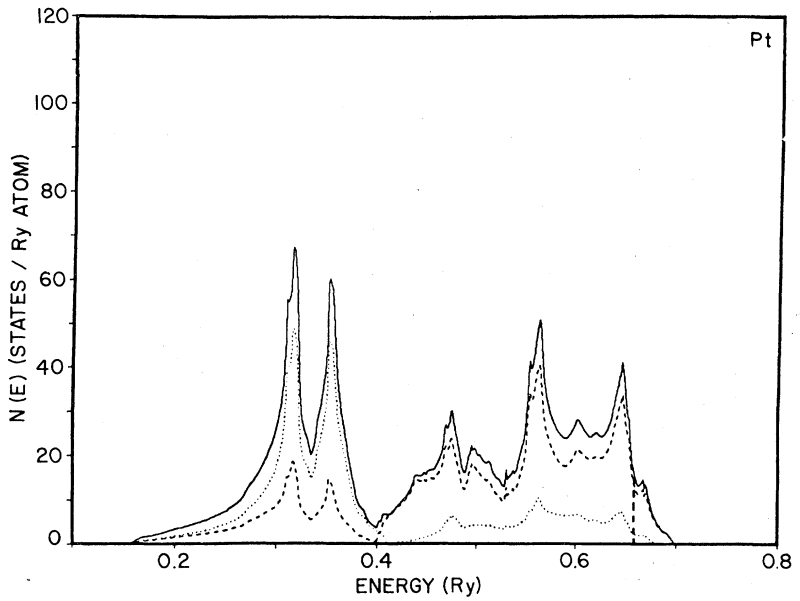

FIG. 5. LCAO density of states $N(E)$ for a simplified calculation involving only the Pt $5d$ bands. Also shown are the projected densities of states $N_{d_{5/2}}(E)$ (dashed) and $N_{d_{3/2}}(E)$ (dotted), respectively. The dashed vertical line is the Fermi energy, assuming 0.3 holes/Pt atom.

bands. The density of states obtained in our previous LCAO $5d$-band calculation for Pt (Ref. 4) is shown in Fig. 5. The Fermi energy, assuming 0.3 holes/atom, is shown by the dashed vertical line. The d-band parameters in this simplified LCAO model are identical with those used in obtaining the full s, p, d LCAO model results of Figs. 1 and 3. Yet the calculated $h_{5/2}/h_{3/2}$ and $N_{d_{5/2}}(E_F)/N_{d_{3/2}}(E_F)$ ratios are about 7. It is evident that hybridization of the Pt $5d$-band states with the overlapping $6s$-$6p$ bands is responsible for reducing this ratio by about a factor of 2.

IV. COMPARISON WITH EXPERIMENT

A. $N_{6,7}$ emission spectra of Pt and Au

The $N_{6,7}$ emission spectra of Pt and Au are useful examples for illustrating the effects of spin-orbit coupling within the $5d$ bands on the calculated spectra. At least two groups have measured the $N_{6,7}$ emission spectra of Pt (Refs. 20 and 21) and Au.[20,22] In analyzing their data, Fomichev *et al.*[20] found that the relative intensities of the $N_6(4f_{5/2})$ to $N_7(4f_{7/2})$ emission bands in Pt and Au are about 1:3, which is significantly different from the statistical ratio (6:8). As we shall show, the effects of spin-orbit coupling within the Pt and Au $5d$ bands are the source of this apparent discrepancy.

For our analysis, we consider the photon-energy-integrated intensity $I_{n'l'j'}$ of emission of photons from an excited hole state $|n'l'j'\rangle$. $I_{n'l'j'}$ is given by

$$I_{n'l'j'} = n_{n'l'j'} k^r_{n'l'j'}, \tag{12}$$

where n is the number of excited states and k^r is the rate constant for radiative decay.

If photons are detected using cw excitation of the sample, then

$$\dot{n}_{n'l'j'} = k^e - n(k^r + k^{nr}) = 0, \tag{13}$$

where k^e and k^{nr} are the excitation and nonradiative decay rates, respectively. The indices $n'l'j'$ are omitted from the right-hand side for brevity. Thus,

$$n_{n'l'j} = k^e/(k^r + k^{nr}). \tag{14}$$

In the limit $k^r \gg k^{nr}$,

$$I_{n'l'j'} \approx k^e, \tag{15}$$

while for $k^r \ll k^{nr}$,

$$I_{n'l'j'} \approx k^e k^r / k^{nr}. \tag{16}$$

Since most x-ray-emission spectra are excited using electrons of energy which is large compared to that of the emitted x rays, one may assume that the probability of creating a low-lying hole state is simply proportional to the statistical weight of that state. Thus, we may take $k^e \propto 2j' + 1$.

X-ray-photoemission-spectroscopy (XPS) measurements[23] indicate that the two components of the $4f$ hole spin-orbit doublet have the same value of k^{nr} in both Pt and Au. This is confirmed in the calculations by McGuire,[24] who also finds that k^r

$\ll k^{nr}$. According to Eq. (16),

$$I_{N_7}/I_{N_6} = \tfrac{4}{3}(k^r_{N_7}/k^r_{N_6}) . \tag{17}$$

The numerator and denominator of Eq. (17) each have the form of the integral over energy of Eq. (4), i.e.,

$$k^r_{n'l'j'} \propto \int \sum_{lj} A^{n'l'j'}_{lj}(E) N_{lj}(E) dE . \tag{18}$$

Furthermore, since the energy separation between the N_6 and N_7 levels is small relative to their mean binding energy, they may be presumed to have very similar radial wave functions. In that case, the radial-dipole integrals of Eqs. (5) and (6) cancel in forming the ratio in Eq. (17). Using Eq. (9) and the substitution $h_j \to n_j$, Eq. (17) reduces to

$$I_{N_7}/I_{N_6} = 20 n_{5/2}/(n_{5/2} + 21 n_{3/2}) . \tag{19}$$

Except in pathological cases where exchange and screening effects in the final state are important, we expect that the energy derivatives of Eqs. (16) and (18) will be valid as well.

Substituting values of n_j from Table II, we find

$$\begin{aligned} I_{N_7}/I_{N_6} &= 1.223 \text{ (Pt)}, \\ I_{N_7}/I_{N_6} &= 1.310 \text{ (Au)} . \end{aligned} \tag{20}$$

Thus, in the limit $k^{nr} \gg k^r$, the ratio of the integrated N_7 and N_6 intensities is very similar to that for the $k^r \gg k^{nr}$ limit, namely, 1.333. However, the results in both limits are in apparent disagreement with the experimental findings of Fomichev *et al.*,[20] who estimate $I_{N_7}/I_{N_6} \approx 3$.

We have calculated the N_6 and N_7 emission spectra for Pt and Au using Eq. (7). More precisely, the unbroadened emission spectra $I^{e0}_{N_6}(\omega)$ and $I^{eo}_{N_7}(\omega)$ contain a factor ω^3 times the expressions for $I_{N_6}(\omega)$ and $I_{N_7}(\omega)$ in Eq. (7), where $\hbar\omega$ is the photon energy. In these calculations, we have assumed that the factors $[R^{n'l'j'}_{lj}(E)]^2$ in Eq. (7) are energy independent and equal in value. These theoretical spectra were then broadened with a Lorentzian function of full width Δ, where

$$\Delta = \Delta_1 + \Delta_2 + \Delta_3[(E_F - E)/(E_F - E_m)]^2 . \tag{21}$$

The three contributions to the broadening include the spectrometer resolution[20] $\Delta_1 = 0.25$ eV, the $4f$ core-level width $\Delta_2 = 0.30$ eV,[11] and a simplified form of energy-dependent final-state Auger broadening[25] with $\Delta_3 = 2.0$ eV.

The results of these calculations are given by the dashed lines in Figs. 6 and 8 for Pt and Au, respectively. Experimental XPS values for the $4f_{7/2}$ and $4f_{5/2}$ binding energies (from Table I of Ref. 11) were used in these calculations. The solid line is the sum of the N_6 and N_7 contributions. These are in excellent agreement with the experimental spectra of Fomichev *et al.*,[20] which are shown as insets to the figures.

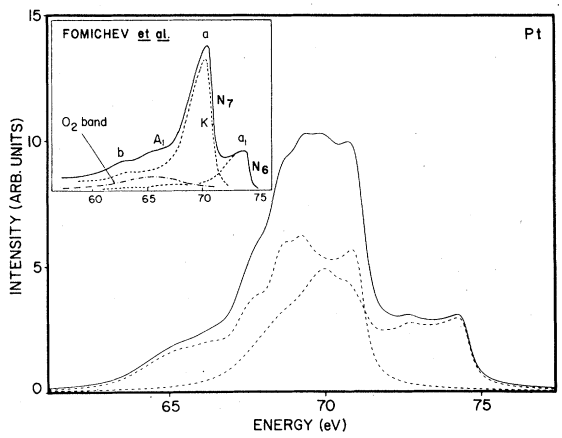

FIG. 6. Comparison of the calculated and observed $N_{6,7}$ emission spectra of Pt.

It is seen that the N_6 spectral density in Pt contains a strong peak which is coincident with the strong peak of the N_7 spectrum. This resolves the dilemma posed by Fomichev *et al.*[20] in regard to the apparent anomolously strong N_7/N_6 intensity ratio.

In order to emphasize the importance of relativistic effects within the $5d$ bands on the general features of the theoretical spectra, we have plotted in Figs. 7 and 9 the corresponding $N_{6,7}$ spectra for Pt and Au in the "nonrelativistic" limit. Namely, we have assumed that $N_d(E) = N_{d_{5/2}} + N_{d_{3/2}}$, $N_{d_{5/2}} = 6N_d/10$, and $N_{d_{3/2}} = 4N_d/10$. It is seen that, in this limit, the N_6 and N_7 spectra have the same shape and are merely shifted in energy by the $4f_{7/2} - 4f_{5/2}$ energy separation.

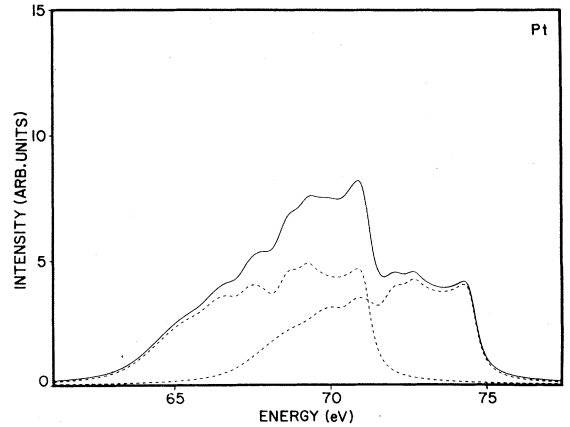

FIG. 7. "Pseudononrelativistic" emission spectrum of Pt, assuming $N_d = N_{d_{5/2}} + N_{d_{3/2}}$, $N_{d_{5/2}} = 0.6\, N_d$, and $N_{d_{3/2}} = 0.4\, N_d$.

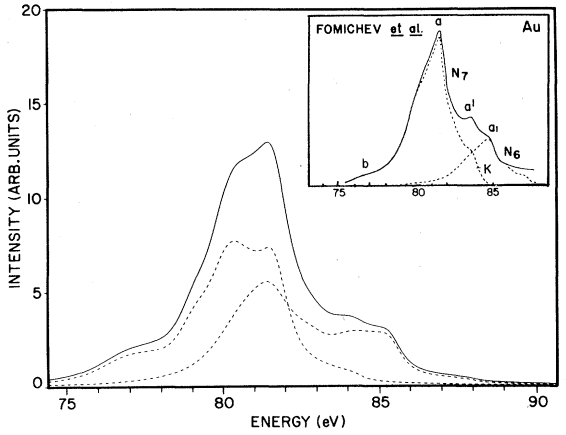

FIG. 8. Comparison of the calculated and observed $N_{6,7}$ emission spectra of Au.

B. $N_{6,7}$ absorption and electron-energy-loss spectra of Pt and Au

In the limit $E_0 \gg \hbar\omega_p$, where E_0 is the energy of a core-electron excitation edge and $\hbar\omega_p$ is the plasmon energy, the photoabsorption spectra (PAS) and the electron-energy-loss spectra (EELS) are very similar. If the dielectric constant $\epsilon(\omega) = \epsilon_1(\omega) + i\epsilon_2(\omega)$, then when $E_0 \gg \omega_p$, $\epsilon_1 \sim 1$ and $\epsilon_2 \ll \epsilon_1$. Under these conditions, the leading term in the absorption coefficient is

$$\mu(\omega) = (2\omega/c)\mathrm{Im}[\epsilon(\omega)^{1/2}] \approx \omega\epsilon_2(\omega)/c\,. \tag{22}$$

Similarly, the probability of observing an energy-loss event for an electron scattered from a crystal is

$$I_L(\omega) \propto \mathrm{Im}[-\epsilon(\omega)^{-1}] \approx \epsilon_2(\omega)\,, \tag{23}$$

where the imaginary part of the dielectric constant $\epsilon_2(\omega)$ is given by

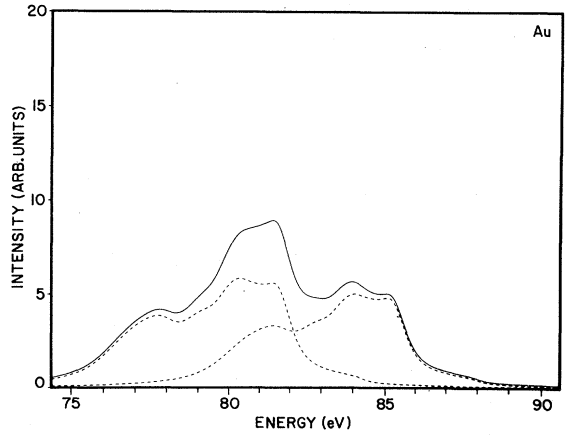

FIG. 9. "Pseudononrelativistic" emission spectrum of Au.

$$\epsilon_2(\omega) = \frac{2\pi^2 e^2\hbar}{m\omega}\sum_{c,\nu}\int \frac{2}{(2\pi)^3}\delta(E_{\nu\vec{k}} - E_c - \hbar\omega) f_{c,\nu\vec{k}}\, d\vec{k}\,, \tag{24}$$

and the interband oscillator strength $f_{c,\nu\vec{k}}$ involving the core state ψ_c with quantum numbers $c \equiv n'l'j'$ and energy E_c is

$$f_{c,\nu\vec{k}} = [2m(E_{\nu\vec{k}} - E_c)/3\hbar^2]\,|\langle\psi_c|\,\vec{r}\,|\psi_{\nu\vec{k}}\rangle|^2\,. \tag{25}$$

Applying the methods summarized in Sec. II B, $\epsilon_2(\omega)$ can be written

$$\epsilon_2(\omega) = \frac{2\pi^2 e^2\hbar N_0}{m\omega}\sum_{lj}(2j'+1)A_{lj}^{n'l'j'}(E)N_{lj}(E)\left(\frac{2m\omega}{3\hbar}\right), \tag{26}$$

where $\hbar\omega = E - E_c \equiv E - E_{n'l'j'}$ and N_0 is the density of atoms/unit volume.

The PAS and EELS spectra are less complicated than the emission spectra in the sense that the initial states of the PAS and EELS spectroscopies are (at least for low-temperature spectra) the electronic ground state. On the other hand, the final states in PAS and EELS are in general a superposition of a number of configurations in which the quantum numbers n, l, j all may vary. This is of particular importance in those cases where the discrete core-excitation edge is separated by a few hundreds of eV or less from the next lower lying (lower binding energy) excitation edge. In these cases the spectra consist of a broad continuum excitation on which is superposed sharp structure due to the core-electron excitation threshold.

It is convenient to consider first the EELS data for the $N_{6,7}$ edge in Au, since the line shape and its interpretation are much simpler than that for Pt and other transition metals. As shown in Fig. 10, the Au EELS data[11] (represented by the open circles) consist essentially of two step functions separated by 3.7 eV and superimposed on a linear background. The $N_6 - N_7$ binding energies E_0 (diamonds) and the core-hole lifetimes Γ are known from XPS data.[23] The solid and dashed lines are fits to the data, assuming that the experimental profile is given by a superposition of step functions convoluted with a Lorentzian whose full width at half maximum (FWHM) is 2Γ. The solid line was determined by adjusting the ratio of the step heights R_{so} so as to yield an optimum fit to the data. This procedure yielded the value $R_{so} = 2.3$. The dashed line corresponds to the value $R_{so} = \frac{4}{3}$, which relates the relative step heights to the degeneracy of the corresponding core-hole state (i.e., $2j'+1$).

The occurrence of this simple EELS line shape in Au is perhaps not unexpected, in view of the $N_{d_{5/2}}(E)$ and $N_{d_{3/2}}(E)$ curves shown in Fig. 4.

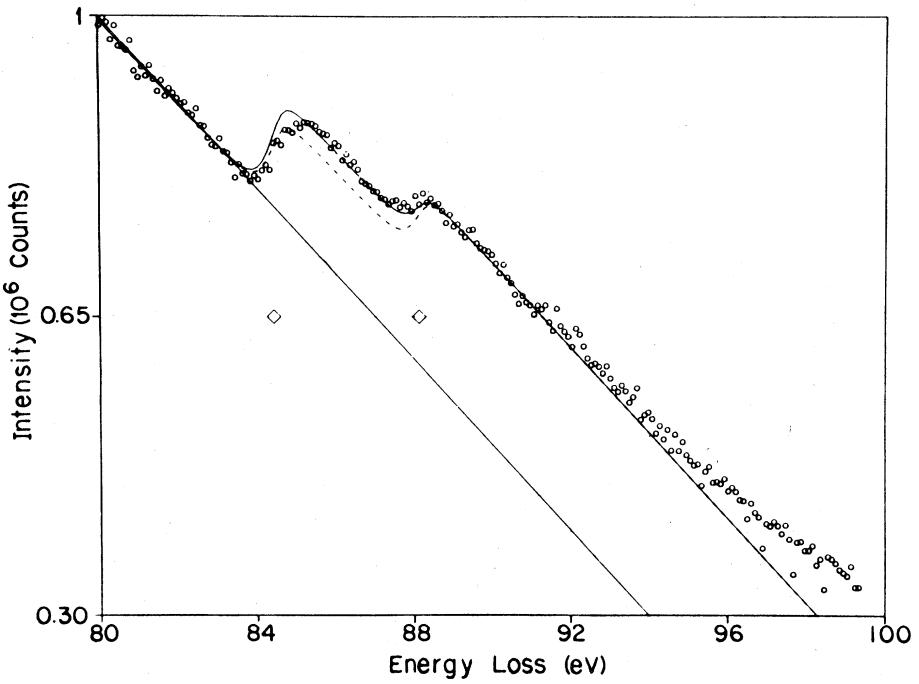

FIG. 10. EELS data for the Au N_6 and N_7 edges (circles) whose XPS binding energies of 88.1 and 84.4 eV, respectively, are marked by diamonds. The solid and dashed lines are theoretical fits which are described in the text.

There, it is found that $N_{d_{5/2}}(E)$ and $N_{d_{3/2}}(E)$ are approximately constant for $E > E_F$. If we denote these constant values by $C_{5/2}$ and $C_{3/2}$, respectively, then according to Eqs. (7) and (9), the step-height ratio

$$R_{so} \equiv I_{N_7}/I_{N_6} = 20/[1 + 21(C_{3/2}/C_{5/2})] = 20/[1 + 21(h_{3/2}/h_{5/2})]. \quad (27)$$

Thus, the observed value $R_{so} = 2.3$ yields an average $h_{5/2}/h_{3/2}$ ratio of 2.7. According to the results of Table II, this is intermediate to the values of 2.4 and 3.0, which correspond to averages over the entire conduction band and within 0.5 eV of E_F, respectively.

In the case of Pt and other transition metals, it has been proposed[26] and demonstrated[26,27] that the PAS and EELS line shapes near threshold for the core-excitation edges with lower binding energies are determined by interferences between the excitation of core electrons into the empty d-band states just above the Fermi level and the excitation of d electrons into continuum states of p and f symmetry. The resulting lines shapes have been shown in favorable cases to be well described as Fano resonances[26,28] in which the continua and discrete final states are mixed by configuration interaction. In spherical symmetry, this implies that continua and discrete states can mix only if they are characterized by the same many-electron total angular momentum J. In cubic or lower symmetry, one may expect that small off-diagonal terms which connect discrete and continua states of different J may exist, but no evidence of this effect has been ascertained as yet.

Of the transition metals, Ni, Pd, and Pt provide the simplest core excitations. The ground states have the approximate configuration $nd^9(n+1)s^1$, where n is, respectively, 3, 4 or 5. The final state in which a core electron of principal quantum number n' and angular momentum l' is excited into the nd band is then $n'l'^{4l'+1}nd^{10}(n+1)s^1$. In the solid the s (or p) conduction electron is not spin polarized, so that we expect only the spin-orbit doublet associated with the $n'l'$ hole multiplet. In this paper we discuss only the $N_{6,7}$ spectra of Pt and Au, but similar behavior has been seen in the $5p$ levels of Au and Pt, and in the $3p$ level of Ni.[11] Detailed analyses of all of these cases have been reported.[11]

In the case of the $4f$ edge in Pt, the ground state is roughly $4f^{14}5s^2\,5p^6\,5d^9\,6s^1\,{}^2D$. The $4f$ excited state is therefore $4f^{13}\,5s^2\,5p^6\,5d^{10}\,6s^1\,{}^2F$. This state is split by the spin-orbit interaction into the $J = \frac{5}{2}$ and $J = \frac{7}{2}$ components. The ^2D ground state contains a superposition of $J = \frac{5}{2}$ and $J = \frac{3}{2}$ with a predominance, according to the results of Sec. III, of $J = \frac{5}{2}$. Thus, for example, one may observe transitions from a $J = \frac{5}{2}$ compo-

nent of ^2D to a $J=\frac{7}{2}$ component of ^2F by exciting a $4f$ electron to the $5d$ band. Similarly, one may reach a different excited state with angular momentum $^2F_{7/2}$ *at the same energy* by exciting a $5d$ electron into a continuum f state, well above the vacuum level. This is a three-particle state consisting of two holes in the $5d$ shell and an electron in ϵf. Since Coulomb and exchange matrix elements connect the discrete and continuum final states, these transitions will interfere with one another.

According to the results in Figs. 3 and 5, the empty $5d$ states in Pt comprise a narrow (~0.3 eV full width at half maximum) spike of states just above E_F. Since this width is of the same order as the broadening of the $4f$ levels due to Auger recombination, it is reasonable to use a simple Fano-type theory for the interference of a single discrete excitation with a degenerate continuum.[28,29] If T_j is the total coherent transition matrix element for component j, then according to Yafet[30]

$$T_j^2(\hbar\omega)=M_j^2\left(\frac{\Gamma_A}{\Gamma_t}+\frac{\Gamma_j}{\Gamma_t}\frac{(q+\epsilon)^2}{\epsilon^2+1}\right), \tag{28}$$

where $\Gamma_t=\Gamma_j+\Gamma_A$, $\epsilon=(\hbar\omega-E_0)/\Gamma_t$, q is an asymmetry parameter, E_0 is the resonance energy, $2\Gamma_t$ is the linewidth in the Lorentzian limit $q\to\pm\infty$, and Γ_j and Γ_A are, respectively, the coherent and Auger (incoherent) contributions to the linewidth. In fitting these line shapes to the data, we also include a contribution to Γ_t of 0.15 eV to account for the finite empty $5d$-band width. M_j is the continuum matrix element. Expressions for M_j, q and Γ are given in Ref. 29.

Letting S_j be the maximum minus the minimum values of T_j^2, i.e., the maximum excursion of the line, then

$$S_j=\frac{M_j^2\Gamma_j}{\Gamma_t}(q^2+1).$$

In Fig. 11 we plot Eq. (28) with values of the parameters appropriate to the Pt N_7 edge: $E_0=71.2$ eV, $\Gamma=0.3$ eV, $q=0.8$. As seen in the figure, the line profile has a zero near the resonance energy E_0. Such a zero is not observed experimentally due to other components (i.e., $J=\frac{3}{2},\frac{5}{2}$) of the continuum which are incoherent with the N_7 edge. Since the linewidth is narrow relative to E_0, it is also a good approximation to assume that M, q, E_0, and Γ are all energy independent. In Pt, the background or continuum spectrum is observed to fluctuate in the vicinity of $N_{6,7}$. This is mainly due to the presence, some 8 eV below the $N_{6,7}$ threshold, of the N_2 resonance, which is probably incoherent with $N_{6,7}$, and to the $5d$ electron Compton scattering

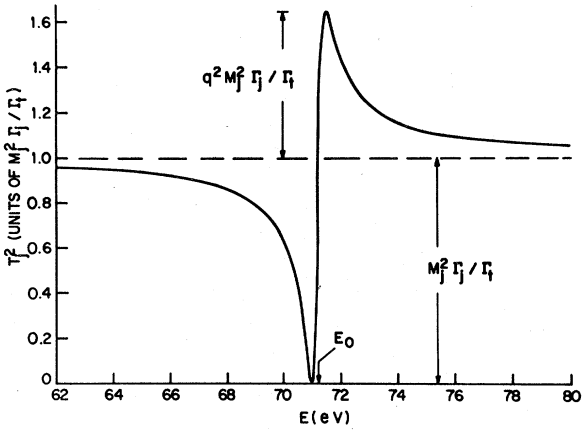

FIG. 11. Plot of the PAS or EELS line shape near the Pt N_7 edge given by the simple Fano theory in Eq. (28).

which diminishes gradually with increasing energy.

In Figs. 12 and 13 we give, respectively, EELS and PAS data for Pt, together with calculated profiles as reported and discussed in Ref. 11. The solid lines were obtained by fitting the peak height ratio R_{so} to the data. The dashed lines were computed assuming $R_{so}=\frac{4}{3}$. The measured ratio was $R_{so}=2.5$ for the EELS data and $R_{so}=2.3$ for the PAS data. The main difference between the EELS and PAS spectra is that the resolution function for the EELS data is ~0.5 eV, whereas it is about 0.03 eV for the PAS data. R_{so} was measured from the maximum excursions of the N_7 and N_6 lines, which we believe to be quite insensitive to the details of the background structure.

It can be shown[29] that q and Γ_t have the same values for both $j_+=l+\frac{1}{2}$ and $j_-=l-\frac{1}{2}$ spin-orbit components by neglecting cubic crystal field splitting of the $4f$ levels and assuming that the radial parts of the j_+ and j_- matrix elements are equal. The equality of Γ_t for the two levels is well supported by XPS data[23] on Pt $N_{6,7}$ emission, which shows that the linewidths are the same to better than 10% and the peak heights stand in ratio 4:3 within an accuracy of order 1%. It follows that

$$\frac{S_{7/2}}{S_{5/2}}=\frac{M_{7/2}^2\Gamma_{7/2}}{M_{5/2}^2\Gamma_{5/2}}.$$

In general M_j is not proportional to P_j, the discrete core-excitation matrix element, and Γ_j differs for different j. However, even for a realistic situation like the present where a number of coherent continua contribute to M_j, it is possible to show[29] that $M_j^2\Gamma_j=P_j^2/\pi q^2$ so that $S_{7/2}/S_{5/2}=P_{7/2}^2/P_{5/2}^2$. Since it follows from sum rules[28]

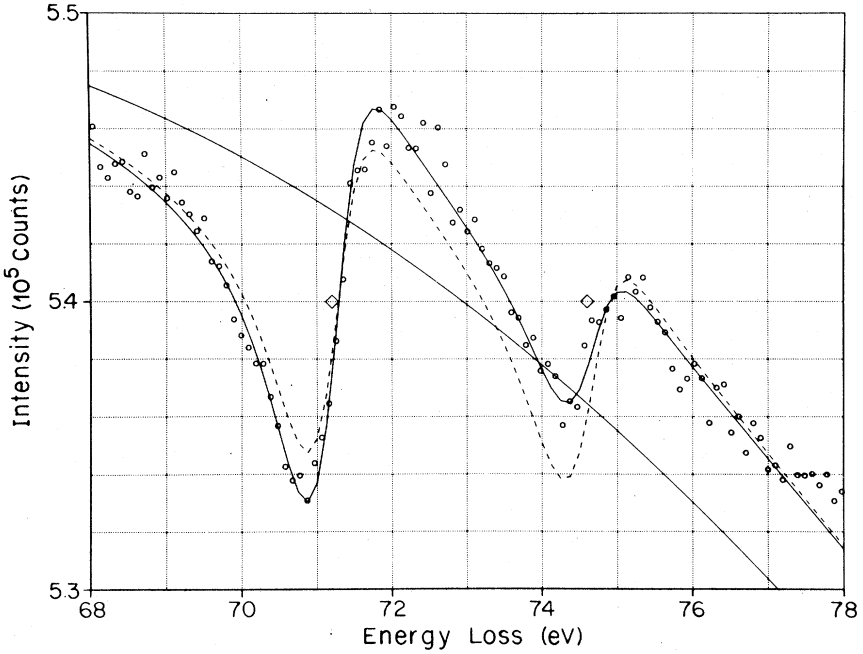

FIG. 12. EELS data for the Pt N_6 and N_7 edges (circles). The dashed and solid curves are fits using N_7/N_6 intensity ratios of 1.33 and 2.5, respectively.

that the integrated area corresponding to the additional oscillator strength for each component is proportional to P_j^2, we have

$$S_{7/2}/S_{5/2} = I_{N_7}/I_{N_6} = 20h_{5/2}/(h_{5/2} + 21h_{3/2}).$$

Taking values for h_j given in Table II we find $R_{so} = I_{N_7}/I_{N_6} = 2.4$ for the total integrated spectral weights, and $R_{so} = 2.9$ for the weights near E_F.

To summarize, the contributions of the 5d band

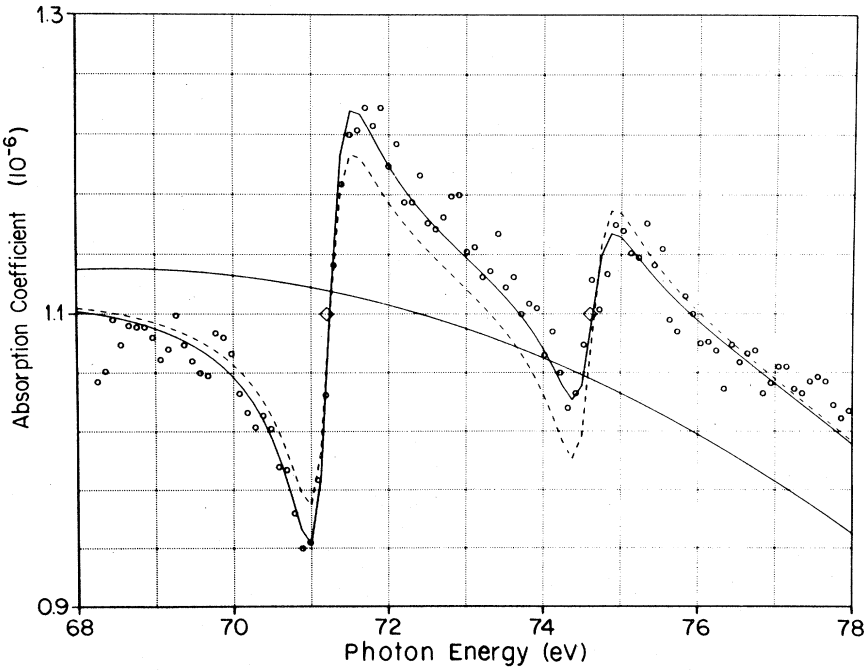

FIG. 13. Absorption data for the N_6 and N_7 excitation edges in Pt. The dashed and solid curves are fits using N_7/N_6 intensity ratios of 1.33 and 2.3, respectively.

structure in Pt relative to the atomic limit are rather subtle in EELS and PAS if one considers only the line shapes: The width of the unoccupied part of the $5d$ band is as narrow as predicted by band theory, but the actual shape of the unoccupied density of states cannot be accurately determined because of core-level lifetime and experimental resolution broadening. The parameter that is both sensitive to the band structure and accurately determined by experiment is the relative intensity of the spin-orbit components R_{so}. For the $N_{6,7}$ edge in Pt, R_{so} must take a value between $\frac{4}{3}$ and $\frac{20}{1}$, depending on whether the $5d$-band width is large or small relative to the $5d$ spin-orbit splitting. The value observed is $R_{so}=2.3$ in PAS and 2.5 in EELS, which is intermediate between the absolute limits for R_{so} and is in excellent agreement with our band-theory calculation. Similar agreement is obtained for the Au $N_{6,7}$ edge.

C. $L_{2,3}$ absorption spectra of Pt

An important feature of the $N_{6,7}$ absorption and emission spectra of Pt and Au is the fact that the N_7-N_6 splitting is small (~5%) compared to the mean binding energy. As a result, one expects the radial wave functions for these spin-orbit doublets to be quite similar and the corresponding radial dipole-moment integrals in Eq. (6) to be nearly equal for each component. These factors then approximately cancel in the analysis of the PAS and EELS data, where the ratio of N_7 and N_6 components is determined.

The $L_{2,3}$ absorption spectra of Pt is less favorable in this respect, since the L_3-L_2 splitting has increased to 14% of the mean binding energy. However, as noted earlier, the L_2 and L_3 absorption-edge data in Pt are rather unique and of considerable theoretical interest in that the L_3 edge exhibits a strong "white line," whereas the L_2 edge does not.[2,3]

Brown *et al.*[3] (BPS) have applied a simplified tight-binding model involving only the Pt $5d$ bands to explain this phenomenon. One striking feature of their calculation is that, assuming 0.3 holes/atom in the Pt $5d$ bands, it predicts $h_{5/2}/h_{3/2}\approx 14$. While they find that this result is consistent with their interpretation of the $L_{2,3}$ absorption spectra, it is clearly inconsistent with the results of the analysis of the Pt $N_{6,7}$ PAS and EELS that is presented in the preceding section. It is therefore of some interest to determine the sensitivity of their analysis to the calculated $h_{5/2}/h_{3/2}$ ratio.

BPS find that if they shift the L_2 absorption-edge data until it is aligned with the L_3 edge and then renormalize it by a factor of 2.22, the two curves coincide at energies 40 eV beyond the aligned edges. The experimental result A_{expt} which they calculate is the area between the L_3 and L_2 absorption curves within 30–40 eV of the edge. They argue that this procedure compensates for multiple-electron excitations as well as possible skewing of the absorption line caused by Fano-type resonances.

Denoting the absorption coefficient $\mu(E)$ near the L_2 and L_3 edges by $\mu_{L_2}(E)$ and $\mu_{L_3}(E)$, respectively, then

$$A_{expt}=\int[\mu_{L_3}(E)-2.22\mu_{L_2}(E)]dE\,,$$
$$=1.11\times10^4\ \text{cm}^{-1}\,\text{eV}\,. \tag{29}$$

However, we have found that a graphical integration of this area in Fig. 5 of their paper indicates that a more accurate value for A_{expt} is about 50% larger than their quoted result, namely, $A_{expt}\approx 1.68\times10^4\ \text{cm}^{-1}\,\text{eV}$.

Actually, BPS calculate only the total L_3 absorption

$$A_{L_3}=\int\mu_{L_3}(E)dE=\frac{2\pi^2e^2\hbar N_0}{mc}\bar{f}_{c,\nu\vec{k}}h_d\,, \tag{30}$$

where N_0 is the number of Pt atoms per unit volume and $\bar{f}_{c,\nu\vec{k}}$ is the average of the oscillator strength [Eq. (25)] over the $(2j'+1)$ core-level $m_{j'}$ values. They then compare this with $A_{expt}(1+h_{3/2}/h_{5/2})$, where the factor $(1+h_{3/2}/h_{5/2})=(1+\frac{1}{14})$ is an approximate correction term for estimating the weak "white line" weight at the L_2 edge.

Using the analysis[7,8] summarized in the preceding sections, it is straightforward to write general expressions for the one-electron contributions to $\mu(E)$ near the L_2 and L_3 absorption edges. However, in the spirit of the BPS calculation, we adopt a more qualitative approach in this discussion. Following BPS, we neglect transitions to $6s$-band final states, since both the density of states and the radial dipole-moment matrix element are about an order of magnitude smaller than that for the $5d$-band final states. If we also neglect the differences between the $R_{d_{5/2}}(r,E)$ and $R_{d_{3/2}}(r,E)$ radial functions and their slight energy dependence over the width of the unfilled $5d$ band, then the following expressions for the integrated absorption coefficient near the L_2 and L_3 edges are obtained:

$$A_{L_2}\equiv\int\mu_{L_2}(E)dE=\frac{2\pi^2e^2\hbar N_0}{mc}\,\frac{2m\hbar\omega_{L_2}}{3\hbar^2}\,(R_d^{2p_{1/2}})^2\frac{h_{3/2}}{3}\,,$$
$$A_{L_3}\equiv\int\mu_{L_3}(E)dE=\frac{2\pi^2e^2\hbar N_0}{mc}\,\frac{2m\hbar\omega_{L_3}}{3\hbar^2}\,(R_d^{2p_{3/2}})^2 \tag{31}$$
$$\times\frac{(6h_{5/2}+h_{3/2})}{15}\,.$$

From Eq. (31) it is clear that $A_{\text{expt}} \equiv A_{L_3} - 2.22A_{L_2}$ is sensitive not only to $5d$ conduction-band properties [the last factors in Eq. (31)], but also to differences in $(R_d^{2p_{3/2}})^2$ and $(R_d^{2p_{1/2}})^2$. The latter effect could be significant in Pt, since the L_3 and L_2 core states differ in energy by ~1700 eV.

BPS neglect these differences and evaluate $R_d^{2p_{3/2}}$ using nonrelativistic Herman–Skillman atomic wave functions. They include relaxation effects by using a Au-atom final state in this calculation. Using the Wigner–Seitz radius for the upper limit of integration in Eq. (6), then $R_{5d}^{2p} = 3.103 \times 10^{-11}$ cm. If we assume $R_{5d}^{2p} = R_d^{2p_{1/2}} = R_d^{2p_{3/2}}$ in Eq. (31), then we can apply the present relativistic LCAO model for Pt to estimate A_{expt}.

For Pt, $N_0 = 0.112 \times 10^{24}$ atoms/cm^3, and the L_2 and L_3 binding energies are 13 273 eV and 11 564 eV, respectively. Evaluating Eq. (31) with these values (plus $h_{5/2} = 1.000$ and $h_{3/2} = 0.344$ from Table II) yields the theoretical result $A_{\text{theor}} = 1.57 \times 10^4$ cm^{-1} eV. This is in surprisingly good agreement with the experimental result $A_{\text{expt}} = 1.68 \times 10^4$ cm^{-1} eV. On the other hand, $A_{\text{theor}} = 1.15 \times 10^4$ cm^{-1} eV when $h_{5/2} = 0.28$ and $h_{3/2} = 0.02$, as determined in the BPS calculation.

In summary, we have noted that serious errors can arise if unjustified assumptions are utilized in evaluating $A_{\text{theor}} = A_{L_3} - 2.22A_{L_2}$ using Eq. (31). However, even in its most simplified form, A_{theor} is relatively insensitive to the $h_{5/2}/h_{3/2}$ ratio. In particular, we have found that increasing the $h_{5/2}/h_{3/2}$ ratio by 480% changes A_{expt} by only 30%.

V. SUMMARY AND CONCLUSIONS

We have shown that core-to-valence-electron excitations in x-ray emission, absorption, and electron energy-loss spectra provide useful probes for determining the total angular-momentum character $j = l \pm \frac{1}{2}$ of the conduction bands. The principle of the method relies on the fact that in favorable cases either the initial (as in Pt and Au emission spectra) or final (as in Pt and Au absorption spectra) states of a core-electron excitation can be usefully characterized as eigenstates of the total angular momentum j. Because the selection rules for dipole transitions also depend on the total angular momentum, the resulting spectral densities are simply linear superpositions of the j projections from the conduction-band densities of states. Thus the spectral densities of the two spin-orbit components of an orbitally degenerate core level will in general be different unless the conduction-band spin-orbit energy $\frac{1}{2}(2l+1)\zeta$ is small compared to the total conduction-band width.

The $N_{6,7}$ spectra of Pt and Au are particularly favorable for illustrating these effects. Not only is the spin-orbit energy of the $5d$ band comparable to its width in these metals, but the $4f$ core-hole lifetime is small relative to the $4f$ spin-orbit splitting, and the $4f$ splitting itself is small relative to the $4f$ binding energy. These considerations allow us to calculate the spectral densities of the individual N_6 and N_7 excitations and their relative intensities, which we find to be in excellent agreement with recently published spectra for both Pt and Au.

We also show that previous attempts to interpret such spectra have been deficient, either because they did not employ a fully relativistic treatment or because they omitted s-p-d hybridization in calculating the conduction-band density of states.

ACKNOWLEDGMENTS

We wish to thank Y. Yafet for many helpful and interesting discussions regarding this work.

[1] N. F. Mott, Proc. Phys. Soc. London 62A, 416 (1949).
[2] Y. Cauchois and I. Manescu, C. R. Acad. Sci. 210, 172 (1940).
[3] M. Brown, R. E. Peierls, and E. A. Stern, Phys. Rev. B 15, 738 (1977).
[4] R. E. Dietz, L. F. Mattheiss, and J. H. Weaver, in *Transition Metals, 1977,* edited by M. J. G. Lee, J. M. Perz, and E. Fawcett (Institute of Physics, Bristol and London, 1978), p. 145.
[5] J. C. Slater and G. F. Koster, Phys. Rev. 94, 1498 (1954).
[6] N. V. Smith, Phys. Rev. B 9, 1365 (1974).
[7] P. Weinberger and F. Rosicky, Theor. Chim. Acta 48, 349 (1978).
[8] L. F. Mattheiss and Y. Yafet (unpublished).
[9] F. Herman and S. Skillman, *Atomic Structure Calculations* (Prentice-Hall, Englewood Cliffs, 1963).
[10] N. E. Christensen, J. Phys. F 8, L51 (1978).
[11] R. E. Dietz, E. G. McRae, and J. H. Weaver, Phys. Rev. B 21, 2229 (1980).
[12] E. U. Condon and G. H. Shortley, *Theory of Atomic Spectra* (Cambridge University Press, London, 1953).
[13] O. Jepson and O. K. Andersen, Solid State Commun. 9, 1763 (1971); G. Lehmann and M. Taut, Phys. Status Solidi B 54, 469 (1972).
[14] N. V. Smith, G. K. Wertheim, S. Hüfner, and M. M. Traum, Phys. Rev. B 10, 3197 (1974).
[15] It is noted that Eqs. (4)–(6) can be applied to the relativistic APW or KKR methods if $R_{lj}(r, E)$ is normalized to unity within each APW sphere of radius R.
[16] A full tabulation of the LCAO parameters for Pt and Au is available from the authors upon request.

[17]O. K. Andersen, Phys. Rev. B 2, 883 (1970).
[18]N. E. Christensen and B. O. Seraphin, Phys. Rev. B 4, 3321 (1971).
[19]F. M. Mueller, J. W. Garland, M. H. Cohen, and K. H. Bennemann, Ann. Phys. 67, 19 (1971).
[20]V. A. Fomichev, T. M. Zimkina, A. V. Rudnev, and S. A. Nemnonov, in *Band Structure Spectroscopy of Metals and Alloys*, edited by D. J. Fabian and L. M. Watson (Academic, New York, 1973).
[21]R. C. Dobbyn, A. J. McAlister, J. R. Cuthill, and N. E. Erickson, Phys. Lett. 47A, 251 (1974).
[22]A. J. McAlister, M. L. Williams, J. R. Cuthill, and R. C. Dobbyn, Solid State Commun. 9, 1775 (1971).
[23]Y. Yafet and G. K. Wertheim, J. Phys. F 7, 357 (1977).
[24]E. J. McGuire, Sandia Laboratories Report No. SC-RR-710835 (unpublished).
[25]D. A. Goodings and R. Harris, J. Phys. C 2, 1808 (1969).
[26]R. E. Dietz, E. G. McRae, Y. Yafet, and C. W. Caldwell, Phys. Rev. Lett. 33, 1372 (1974).
[27]L. C. Davis and L. A. Feldkamp, Solid State Commun. 19, 413 (1976).
[28]U. Fano, Phys. Rev. 124, 1866 (1961).
[29]G. P. Williams, G. J. Lapeyre, F. Cerrina, I. T. McGovern, R. E. Dietz, and Y. Yafet (unpublished).
[30]Y. Yafet, Phys. Rev. B 21, 5023 (1980).